

Probing Heavy Charged Higgs Boson Using Multivariate Technique at Gamma-Gamma Collider

Ijaz Ahmed,^{1,*} Abdul Quddus,^{1,†} Jamil Muhammad,^{2,‡}

Muhammad Shoaib,^{3,§} and Saba Shafaq^{4,¶}

¹*Federal Urdu University of Arts, Science and Technology, Islamabad Pakistan*

²*Sang-Ho College, and Department of Physics,
Konkuk University, Seoul 05029, South Korea*

³*Institute of Physics (IoP), The Islamia University of Bahawalpur, Bahawalpur 63100, Pakistan*

⁴*International Islamic University Islamabad Pakistan*

(Dated: April 1, 2024)

Abstract

The current study explores the production of charged Higgs particles through photon-photon collisions within the Two Higgs Doublet Model context, including one-loop-level scattering amplitude of Electroweak and QED radiation. The cross-section has been scanned for plane (m_{ϕ^0}, \sqrt{s}) investigating the process of $\gamma\gamma \rightarrow H^+H^-$. Three particular numerical scenarios low- m_H , non-alignment, and short-cascade are employed. Hence using h^0 for low- m_{H^0} and H^0 for non-alignment and short-cascade scenario, the new experimental and theoretical constraints are applied. The decay channels for charged Higgs particles are examined in all the scenarios along with the analysis for cross-sections revealing that at low energy it is consistently higher for all scenarios. However, as \sqrt{s} increases, it reaches a peak value at 1 TeV for all benchmark scenarios. The branching ratio of the decay channels indicates that for non-alignment, the mode of decay $W^\pm h^0$ takes control and for short cascade, the prominent decay mode remains $t\bar{b}$, while in the low- m_H the dominant decay channel is of $W^\pm h^0$. In our research, we employ contemporary machine-learning methodologies to investigate the production of high-energy Higgs Bosons within a 3TeV Gamma-Gamma collider. We have used multivariate approaches such as Boosted Decision Trees (BDT), LikelihoodD, and Multilayer Perceptron (MLP) to show the observability of heavy-charged Higgs Bosons versus the most significant Standard Model backgrounds. The purity of the signal efficiency and background rejection are measured for each cut value.

PACS numbers: 12.60.Fr, 14.80.Fd

Keywords: LHC, CMS, Charged Higgs, 2HDM, Gamma-Gamma Collider, Multivariate, ILC, CLIC, ANN.

*Electronic address: ijaz.ahmed@fuuast.edu.pk

†Electronic address: abdulqudduskakakhail@gmail.com

‡Electronic address: mjamil@konkuk.ac.kr

§Electronic address: muhammad.shoaib@iub.edu.pk

[¶]Electronic address: saba.shafaq@iiu.edu.pk

I. INTRODUCTION

A neutral Higgs boson was discovered by the ATLAS and CMS collaborations at the Large Hadron Collider (LHC) in 2012 having approximately a mass of 125 GeV and its properties were consistent with the prediction of Standard Model (SM) Higgs [1–3]. Within the SM framework, gauge boson acquire their masses due to the Brout–Englert–Higgs mechanism utilizing the concept of electroweak symmetry breaking (EWSB). The SM of particle physics does not provide any indications of charged Higgs bosons. However, theories beyond the SM propose the existence of charged Higgs bosons and are frequently incorporated into theoretical frameworks such as Two-Higgs-Doublet Models (2HDM), supersymmetric models, composite Higgs models grand unified theories, and axion models. Among all these BSM theories, the two Higgs doublet model is very important due to its structural relevance to many new physics models like MSSM [4, 5], composite Higgs models, axion models [6, 7]. Depending upon the couplings to the quarks, the types of 2HDMs predict different properties and interactions for charged Higgs bosons. A charged Higgs boson would be a more massive counterpart to the SM W^\pm and Z bosons, which are carriers of the weak force. The Higgs sector in 2HDM is extended to incorporate other degrees of freedom that include the prediction of five Higgs candidates of the minimal supersymmetric extension of the SM (MSSM) [8, 9]. From these five Higgs boson candidates, two are CP even neutral states h , H , one is CP odd A state and the remaining two states charge Higgs states H^\pm . The discovery of any new scalar Higgs boson either neutral or charged will be a strong hint towards the physics beyond the SM of particle physics and the immediate sign of an extended Higgs sector.

The future e^+e^- and $\gamma\gamma$ -colliders, with high energy and luminosity, offer a great potential for discovering charged Higgs boson. The output rate at a $\gamma\gamma$ -collider could exceed that of e^+e^- -collisions at the tree level. In 2HDM, the $e^+e^- \rightarrow H^+H^-$ process has been analyzed at the tree level, while the $\gamma\gamma \rightarrow H^+H^-$ process was only studied at the Born level with Yukawa corrections [10, 11]. Due to the s-channel contribution the $e^+e^- \rightarrow H^+H^-$ triumphs over the cross-section, so the rate of production of $\gamma\gamma \rightarrow H^+H^-$ is higher than the $e^+e^- \rightarrow H^+H^-$. The scattering process of $\gamma\gamma \rightarrow H^+H^-$ has been studied at the one-loop level.

This paper will focus on the multivariate analysis of charged Higgs boson production at the photon-photon collider at the International Linear Collider (ILC). Three benchmark points are selected for numerical examination, each with a \mathcal{CP} -even scalar mass of 125 GeV and couplings consistent with the known Higgs boson. These points are derived from the “non-alignment”, “low- m_H ”, and “short-cascade” scenarios, and have been accurately delineated within the constraints of current

experimental data and are fully consistent with theoretical constraints [12]. The cross-section is scanned for plane (ϕ^0, \sqrt{s}) , where ϕ^0 is h^0 for low- m_H and H^0 for non-alignment and short-cascade scenarios. Additionally, the polarization effect is also discussed for all scenarios.

II. REVIEW OF TWO HIGGS DOUBLET MODEL

The two scalar doublets are used to acquire masses for gauge bosons and fermions after having their vacuum expectation values (VEVs). The Lagrangian is given by:

$$\mathcal{L}_{2HDM} = \mathcal{L}_{SM} + \mathcal{L}_{Scalar} + \mathcal{L}_{Yukawa} \quad (1)$$

Where \mathcal{L}_{Scalar} is the Lagrangian for two scalar doublets including kinetic term and scalar potential terms. The Z_2 symmetry is involved to ignore the Flavour Changing Neutral currents (FCNCs), then the transformation for even, $\Phi_1 \rightarrow +\Phi_1$, and for odd is $\Phi_2 \rightarrow -\Phi_2$. To keep \mathcal{L}_{Yukawa} invariant for fermions under Z_2 -symmetry the fermions are coupled with one scalar field:

$$\mathcal{L}_{Yukawa} = -\bar{Q}_L Y_u \tilde{\Phi}_u u_R - \bar{Q}_L Y_d \Phi_d d_R - \bar{L}_L Y_\ell \Phi_\ell \ell_R + h.c \quad (2)$$

In Equation 2 the $\Phi_{u,d,\ell}$ is either Φ_1 or Φ_2 , so based on the discrete symmetry of fermions the 2HDM is classified into four types called as Type-I, II, III, and IV. The review for this relevant study is discussed here for \mathcal{CP} -conserving 2HDM. If we assume that in the 2HDM the electromagnetic gauge symmetry is present to perform $SU(2)$ rotation on two doublets for alignment of VEVs of two doublets with $SU(2)$ and the $v = 246 \text{ GeV}$ will occupy one neutral Higgs doublet [13]. The two complex doublets, Φ_1 from SM and Φ_2 from EW symmetry-breaking are used to construct the 2HDM. The scalar potential under $SU(2)_L \otimes U(1)_Y$ invariant gauge group is defined as

$$\begin{aligned} V_{2HMD} = & m_1^2 |\Phi_1|^2 + m_2^2 |\Phi_2|^2 - \left[m_{12}^2 (\Phi_1^\dagger \Phi_2) + h.c \right] + \frac{\lambda_1}{2} (\Phi_1^\dagger \Phi_2)^2 + \frac{\lambda_2}{2} (\Phi_2^\dagger \Phi_1)^2 \\ & + \lambda_3 (\Phi_1^\dagger \Phi_1) (\Phi_2^\dagger \Phi_2) + \lambda_4 (\Phi_1^\dagger \Phi_2) (\Phi_2^\dagger \Phi_1) + \left[\frac{\lambda_5}{2} (\Phi_1^\dagger \Phi_2)^2 + \lambda_6 (\Phi_1^\dagger \Phi_1) (\Phi_1^\dagger \Phi_2) \right. \\ & \left. + \lambda_7 (\Phi_1^\dagger \Phi_2) (\Phi_2^\dagger \Phi_2) + h.c \right] \end{aligned} \quad (3)$$

In the above Equation 3 the quartic coupling parameters are λ_i ($i = 1, 2, 3, \dots, 7$) and the complex two doublets are Φ_i ($i = 1, 2$). Hermiticity of the potential forces $\lambda_{1,2,3,4}$ to be real while $\lambda_{5,6,7}$ and m_{12}^2 can be complex. The Paschos-Glashow-Weinberg theorem suggests that a discrete Z_2 -symmetry can explain certain low-energy observables [14, 15]. Utilizing this symmetry is crucial to effectively prevent any possibility of FCNCs occurring at the tree level. The Z_2 -symmetry requires

that $\lambda_6 = \lambda_7 = 0$ and also $m_{12}^2 = 0$. If this is not allowed i.e. m_{12}^2 is non-zero then the Z_2 -symmetry is softly broken for the translation of $\Phi_1 \rightarrow +\Phi_1$ and $\Phi_2 \rightarrow -\Phi_2$. The Z_2 assignments produce four 2HDM-types as mentioned earlier [16, 17]. Table I demonstrates how fermions bind to each Higgs doublet in the permitted kinds when flavor conservation is naturally observed.

Type	u_i	d_i	ℓ_i
I	Φ_2	Φ_2	Φ_2
II	Φ_2	Φ_1	Φ_1
III	Φ_2	Φ_2	Φ_1
IV	Φ_2	Φ_1	Φ_2

TABLE I: In 2HDMs with Z_2 -symmetry, Higgs doublets Φ_1, Φ_2 couple to u-type and d-type quarks, as well as charged leptons.

This work focuses only on Type-I and Type-II 2HDM whereas in Type-I only Φ_2 doublet interacts with both quarks and lepton similarly as SM. In Type-II the Φ_1 couples with d-type quarks and leptons while the Φ_2 with only u-type quarks.

After electroweak symmetry breaking of $SU(2)_L \otimes U(1)_Y$, the scalar doublet's neutral components gets VEV to be v_j .

$$\Phi_j = \begin{pmatrix} \phi_j^+ \\ \frac{1}{\sqrt{2}}(v_j + \rho_j + i\eta_j) \end{pmatrix}, \quad (j = 1, 2) \quad (4)$$

where ρ_j and η_j are real scalar fields. The quartic coupling parameters $\lambda_1 - \lambda_5$ and mass terms m_1^2, m_2^2 are considered as physical masses of m_h, m_H, m_A, m_{H^\pm} with $\tan \beta = \frac{v_1}{v_2}$ and mixing term $\sin(\beta - \alpha)$. After Z_2 -symmetry is broken softly the parameter m_{12}^2 is given by

$$m_{12}^2 = \frac{1}{2} \lambda_5 v^2 \sin(\beta - \alpha) \cos(\beta - \alpha) = \frac{\lambda_5}{2\sqrt{2}G_F} \left(\frac{\tan \beta}{1 + \tan^2 \beta} \right) \quad (5)$$

where the last equality is only for the tree level. By considering λ_6 and λ_7 equal to zero concerning Z_2 -symmetry, m_{12}^2 , $\tan \beta$ and mixing angle α with four Higgs mass is enough to compute a complete model in physical basis. So, with all this, there are seven independent free parameters to explain the Higgs sector in 2HDM. The terms m_1^2 and m_2^2 are given in the form of other parameters:

$$m_1^2 = m_{12}^2 \frac{v_2}{v_1} - \frac{\lambda_1}{2} v_1^2 - \frac{1}{2} (\lambda_3 + \lambda_4 + \lambda_5) v_2^2 \quad (6)$$

$$m_2^2 = m_{12}^2 \frac{v_1}{v_2} - \frac{\lambda_1}{2} v_1^2 - \frac{1}{2} (\lambda_3 + \lambda_4 + \lambda_5) v_2^2 \quad (7)$$

The phenomenology is dependent upon the mixing angle with angle β . In the limit where \mathcal{CP} -even Higgs boson h^0 acts like SM Higgs then it approaches the non-alignment limit which is most favored by experimentalists if $\sin(\beta - \alpha) \rightarrow 1$ or $\cos(\beta - \alpha) \rightarrow 0$. The H^0 acts as gauge-phobic such that its coupling with vector bosons Z/W^\pm is much more suppressed, but when $\cos(\beta - \alpha) \rightarrow 1$ the H^0 acts SM-like Higgs boson. For the decoupling limits $\cos(\beta - \alpha) = 0$ and $m_{H^0, A^0, H^\pm} \gg m_Z$ so at this limit h^0 interacts with SM particles completely appears like the couplings of the SM Higgs boson that contain coupling $3h^0$.

III. CONSTRAINTS FROM THEORY AND EXPERIMENT

The theoretical restrictions of potential unitarity, stability, and perturbativity compress the parameter space of the scalar 2HDM potential. The vacuum stability of the 2HDM limits the V_{2HDM} . Specifically, $V_{2HDM} \geq 0$ needs to be met for all Φ_1 and Φ_2 directions. As a result, the following criteria are applied to the parameters λ_i [18, 19]

$$\lambda_1 > 0 \quad , \quad \lambda_2 > 0 \quad , \quad \lambda_3 + \sqrt{\lambda_1 \lambda_2} + \text{Min}(0, \lambda_4 - |\lambda_5|) > 0 \quad (8)$$

Another set of constraints enforces that the perturbative unitarity needs to be fulfilled for the scattering of longitudinally polarized gauge and Higgs bosons. Besides, the scalar potential needs to be perturbative by demanding that all quartic coefficients satisfy $|\lambda_{1,2,3,4,5}| \leq 8\pi$. The global fit to EW requires $\Delta\rho$ to be $\mathcal{O}(10^{-3})$ [20]. This prevents substantial mass splitting between Higgs boson in 2HDM and requires that $m_{H^\pm} \approx m_A, m_H$ or m_h .

Aside from the theoretical restrictions mentioned above, 2HDMs have been studied in previous and continuing experiments, such as direct observations at the LHC or indirect B-physics observables. As a consequence, numerous findings have been amassed since then, and the parameter space of the 2HDM is now constrained by all results obtained. In the Type-I of 2HDM, the following pseudoscalar Higgs mass regions $310 < m_A < 410 \text{ GeV}$ for $m_H = 150 \text{ GeV}$, $335 < m_A < 400 \text{ GeV}$ for $m_H = 200 \text{ GeV}$, $350 < m_A < 400 \text{ GeV}$ for $m_H = 250 \text{ GeV}$ with $\tan\beta = 10$ have been excluded by the LHC experiment [21]. Furthermore, the \mathcal{CP} -odd Higgs mass is bounded as $m_A > 350 \text{ GeV}$ for $\tan\beta < 5$ [22] and the mass range $170 < m_H < 360 \text{ GeV}$ with $\tan\beta < 1.5$ is excluded for the Type-I [23].

The H^\pm mass is constrained by experiments at the LHC and prior colliders, as well as B-physics observables. The $\text{BR}(b \rightarrow s\gamma)$ measurement limits the charged Higgs mass in Type-II and IV 2HDM with $m_{H^\pm} > 580 \text{ GeV}$ for $\tan\beta \geq 1$ [24, 25]. On the other hand, the bound is significantly

lower in Type-I and III of 2HDM [26]. With $\tan \beta \geq 2$, the H^\pm in Type-I and III of 2HDM can be as light as 100 *GeV* [27, 28] while meeting LEP, LHC, and B-physics constraints [29–33].

IV. BENCHMARK POINTS SCENARIOS

We have taken three scenarios [12]: non-alignment, short cascade, and low- m_H . All of these are taken for \mathcal{CP} –even scalar of mass 125 *GeV* and couplings are well arranged with observed Higgs boson. The additional Higgs boson searches leave a considerable portion of their parameter space unconstrained, emphasizing the need for further investigation. Validation of potential stability, perturbativity, and unitarity for each BP was performed using 2HDMC 1.8.0 [34].

These benchmark situations, shown in Table II, are created using a hybrid approach, where the input parameters are specified as $(m_h, m_H, \cos(\beta - \alpha), \tan \beta, Z_4, Z_5, Z_7)$ with softly broken 2HDM of Z_2 –symmetry, where the $Z_{4,5,7}$ are quartic couplings in Higgs basis of $\mathcal{O}(1)$. The mass of charged Higgs and pseudoscalar Higgs in this basis are obtained as:

$$m_{A^0}^2 = m_{H^0}^2 s_{\beta-\alpha}^2 + m_{h^0}^2 c_{\beta-\alpha}^2 - Z_5 v^2 \quad (9)$$

$$m_{H^\pm}^2 = m_{A^0}^2 - \frac{1}{2}(Z_4 - Z_5)v^2 \quad (10)$$

In the **non-alignment scenario**, the lightest \mathcal{CP} –even scalar h^0 , the discovered Higgs boson is interpreted, with SM-like properties. In an alignment scenario heavy \mathcal{CP} –even H^0 could not decay into GB but in a non-alignment scenario it is allowed by present constraints. In this situation to have a H^\pm must satisfy the $b \rightarrow s\gamma$ constraint, and quartic couplings are set to -2. The $\tan \beta$ and m_{H^0} are remain free parameters.

In the **short-cascade scenario** the SM like h^0 is taken exactly to alignment i.e $\cos(\beta - \alpha) = 0$. We considered mass hierarchy such as to decay $H^0 \rightarrow W^\pm H^\pm$ or $H^0 \rightarrow A^0 Z^0$ which results Higgs-to-Higgs decay in small cascade. The Z_7 and $\tan \beta$ are remained fixed parameters.

A **low- m_H scenario** is proposed where both \mathcal{CP} –even Higgs boson (h^0, H^0) are light. The heavier one is assumed to be an SM-like Higgs boson, resulting in $m_{H^0} = 125$ *GeV*. The heavier \mathcal{CP} –even Higgs coupling to gauge bosons is proportional to $\cos(\beta - \alpha)$. Because $m_h < m_H$, the couplings of lighter \mathcal{CP} –even scalars to vector bosons must have been strongly suppressed to comply with direct search limits, forcing $\sin(\beta - \alpha) = 0$. The parameter space for $90 < m_h < 120$ *GeV* is constrained by searches $h \rightarrow b\bar{b}, \tau\tau$ at the LHC, which leads to an upper constraint on $\tan \beta$. The mass hierarchy is considered for these benchmark points along with the type of the 2HDMs, shown in Table III. In Table II, $t_\beta = \tan \beta$ and $c_{\beta-\alpha} = \cos(\beta - \alpha)$.

Scenario	m_{h^0} [GeV]	m_{H^0} [GeV]	$c_{\beta-\alpha}$	Z_4	Z_5	Z_7	t_β
BP-1	125	150...600	0.1	-2	-2	0	1...20
BP-2	125	250...500	0	-1	1	-1	2
BP-3	125	250...500	0	2	0	-1	2
BP-4	65...120	125	1.0	-5	-5	0	1.5

TABLE II: A set of benchmark scenario input parameters that may be utilized to actualize the 2HDM in Hybrid Basis.

Scenarios	BP's	2HDM-Type	Mass Hierarchy
Non-alignment	BP-1	I	$m_{H^0} < m_{H^\pm} = m_{A^0}$
Short Cascade	BP-2	I	$m_{A^0} < m_{H^\pm} = m_{H^0}$
Short Cascade	BP-3	I	$m_{H^\pm} < m_{A^0} = m_{H^0}$
Low-m_H	BP-4	II	$m_{h^0} < m_{H^\pm} = m_{A^0}$

TABLE III: Mass hierarchy for BP's with 2HDM types used in calculations of cross-section and decay width of charged Higgs.

V. THE LEADING ORDER CROSS-SECTION OF CHARGED HIGGS PRODUCTION

Analytical formulations of the cross-section of the e^+e^- collider for charged Higgs pair generation are presented in this section. The process used in this paper is given as:

$$\gamma(k_1, \mu) \ \gamma(k_2, \nu) \longrightarrow H^+(k_3) \ H^-(k_4) \quad (11)$$

where $k_a (a = 1, \dots, 4)$ represent the four momenta. There are three different diagrams at the tree level that are topologically distinct because of photon coupling as shown in Figure 1. The total Feynman amplitude is given by:

$$\mathcal{M} = \mathcal{M}_{\hat{q}} + \mathcal{M}_{\hat{t}} + \mathcal{M}_{\hat{u}} \quad (12)$$

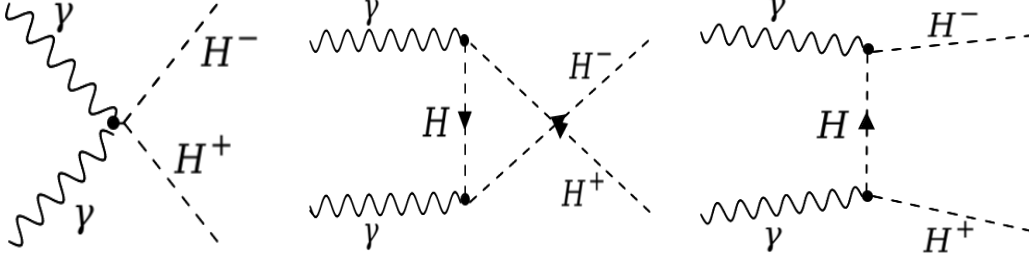


FIG. 1: The tree-level Feynman diagrams for the process $\gamma\gamma \rightarrow H^+H^-$.

where $\mathcal{M}_{\hat{q}}$, $\mathcal{M}_{\hat{t}}$ and $\mathcal{M}_{\hat{u}}$ are amplitudes of quartic couplings, t-channel, and u-channel Feynman diagrams respectively. The relations for these channels are given as follows:

$$\mathcal{M}_{\hat{q}} = 2ie^2 g^{\mu\nu} \epsilon_\mu(k_1) \epsilon_\nu(k_2) \quad (13)$$

$$\mathcal{M}_{\hat{t}} = \frac{ie^2}{\hat{t} - m_{H^+}^2} (k_1 - 2k_4)^\nu \epsilon_\nu(k_2) (k_2 + k_3 - k_4)^\mu \epsilon_\mu(k_1) \quad (14)$$

$$\mathcal{M}_{\hat{u}} = \frac{-ie^2}{\hat{u} - m_{H^+}^2} (k_1 - 2k_4)^\mu \epsilon_\mu(k_1) (k_1 + k_3 - k_4)^\nu \epsilon_\nu(k_2) \quad (15)$$

where the Mandelstam variables are represented by $\hat{t} = (k_1 - k_3)^2$ and $\hat{u} = (k_2 - k_4)^2$. After calculating the square of the total amplitude and summing up the polarization vectors, the expression becomes:

$$|\mathcal{M}|^2 = 256\pi^2\alpha^2 \left[\left(\frac{t}{(t - m_{H^+}^2)^2} + \frac{u}{(u - m_{H^+}^2)^2} - \frac{1}{t - m_{H^+}^2} - \frac{1}{u - m_{H^+}^2} \right) m_{H^+}^2 + \frac{9m_{H^+}^2 - 3m_{H^+}^2(2m_{H^+}^2 + s) + (s+t)(s+u)}{2(t - m_{H^+}^2)(u - m_{H^+}^2)} \right] \quad (16)$$

The scattering amplitude is calculated numerically in the center of the mass frame, where the four-momentum and scattering angle are indicated by (k, θ) . In the center of mass energy, the energy (k_i^0) and momentum (\vec{k}_i) of incoming and outgoing particles are:

$$k_1 = \frac{\sqrt{s}}{2}(1, 0, 0, 1) \quad , \quad k_2 = \frac{\sqrt{s}}{2}(1, 0, 0, -1) \quad (17)$$

$$k_3 = (k_3^0, |\vec{k}| \sin \theta, 0, |\vec{k}| \cos \theta) \quad (18)$$

$$k_4 = (k_4^0, -|\vec{k}| \sin \theta, 0, -|\vec{k}| \cos \theta) \quad (19)$$

$$k_3^0 = \frac{s + m_i^2 - m_j^2}{2\sqrt{s}} \quad , \quad k_4^0 = \frac{s + m_j^2 - m_i^2}{2\sqrt{s}} \quad (20)$$

$$|\vec{k}| = \frac{\lambda(s, m_{H^+}^2, m_{H^-}^2)}{\sqrt{s}} \quad (21)$$

where m_i^2 is the mass of relevant particles. The cross-section is calculated by taking the flux of incoming particles and the integral over the phase space of outgoing particles is given by:

$$\hat{\sigma}_{\gamma\gamma \rightarrow H^+ H^-}(s) = \frac{\lambda(s, m_{H^+}^2, m_{H^-}^2)}{16\pi s^2} \sum_{pol} |M|^2 \quad (22)$$

In above expression the $\lambda(s, m_{H^+}^2, m_{H^-}^2)$ is the Källén function relevant to phase space of outgoing H^\pm . The total integrated cross section for e^+e^- -collider could be calculated by:

$$\sigma(s) = \int_{x_{min}}^{x_{max}} \hat{\sigma}_{\gamma\gamma \rightarrow H^+ H^-}(\hat{s}; \hat{s} = z^2 s) \frac{dL_{\gamma\gamma}}{dz} dz \quad (23)$$

where s and \hat{s} are the C.M energy in e^+e^- -collider and subprocess of $\gamma\gamma$, respectively. The value of x_{min} represents the minimum amount of energy needed to generate a pair of charged Higgs particles and is given by $x_{min} = (m_{H^+} + m_{H^-})/\sqrt{s}$, where the x_{max} is 0.83 [35]. The distribution function of the photon luminosity is:

$$\frac{dL_{\gamma\gamma}}{dz} = 2z \int_{x_{min}}^{x_{max}} \frac{dx}{x} F_{\gamma/e}(x) F_{\gamma/e}\left(\frac{z^2}{x}\right) \quad (24)$$

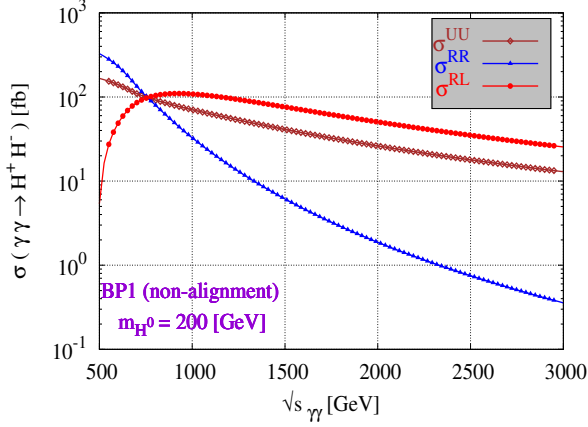
The energy spectrum of Compton back-scattered photons, $F_{\gamma/e}(x)$, is characterized by the electron beam's longitudinal momentum [35].

VI. NUMERICAL RESULTS AND DISCUSSIONS

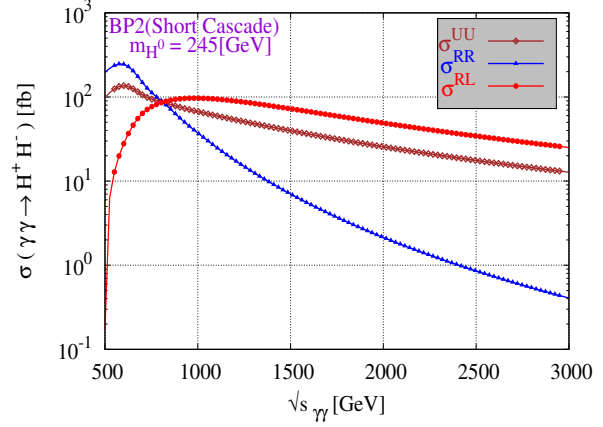
The numerical results of generating charged Higgs boson via photon-photon collisions are thoroughly examined in the context of 2HDM including QED radiations. Cross sections at the tree level are calculated numerically for each benchmark scenario as a function of the C.M energy and the Higgs boson mass. Polarization distributions are presented to improve the production rate by considering longitudinal polarizations of initial beams. Decay pathways of the charged Higgs boson are under study for relevant scenarios.

In our work, for analytical and numerical evaluation we have used **MadGraph5 v3.4.2** [36] for the calculations of the cross-sections, the **2HDMC 1.8.0** [37] for the branching ratio and total decay width. The **GnuPlot** [38] is used for the graphical plotting.

As in Figure 2 the cross-section for the process $\gamma\gamma \rightarrow H^+ H^-$ is shown for the C.M energy of 3 TeV for three types of polarization; right handed RR ($++$), oppositely-polarized RL ($+-$) and unpolarized beam UU . The cross-section is the same for the polarization modes of $\sigma^{+-} = \sigma^{-+}$. In



(a)

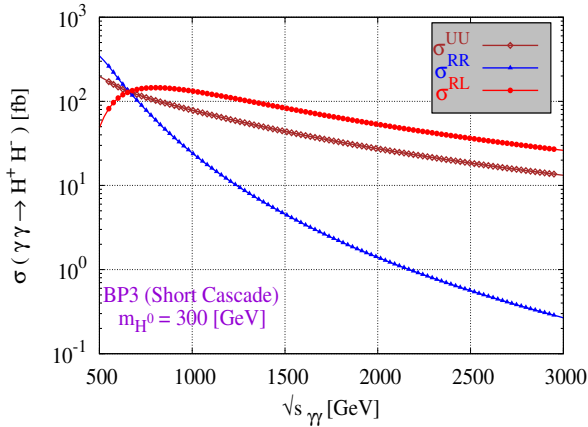


(b)

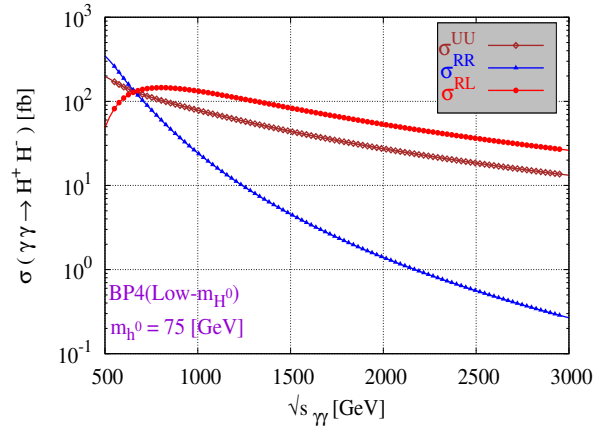
FIG. 2: Integrated cross-section for $\gamma\gamma \rightarrow H^+H^-$ as a function of \sqrt{s} for BP-1 in (a) and BP-2 in (b), respectively

Figure 2 it can be seen that the cross-section is higher for UU and RR for low \sqrt{s} and gradually decreases. But for the RL mode of polarization, the cross-section reaches a peak value and then gradually decreases. As we can see the cross-section is not enhanced for RR and UU at higher energies but it does only for RL .

In Figure 3 for both BPs, the cross-section changes slowly with the mass of h^0 and H^0 because of the small range of charged Higgs mass. For both UU and RR modes of polarization the cross-section decreases with C.M energy and for RL mode it reaches a peak value and then decreases.



(a)



(b)

FIG. 3: Integrated cross-section for process $\gamma\gamma \rightarrow H^+H^-$ as a function of \sqrt{s} for BP-3 in (a) and BP-4 in (b), respectively.

The cross-section σ decreases for \sqrt{s} when $m_{H^\pm} \ll \sqrt{s}/2$.

VII. DECAYS OF CHARGED HIGGS BOSON

The probability that a particular particle will decay per unit time is called decay width. While it is impossible to predict the lifespan of a single particle, a statistical distribution can be determined for a large sample, for this purpose the decay width is used. In this section, we will study the final decay products of the charged Higgs bosons created in all scenarios. To investigate the process in a collider, we must first identify all potentially charged Higgs products. The total decay widths of the charged Higgs boson versus the mass of Higgs h^0 or H^0 are plotted for all BPs. The total rate of decay per unit time Γ is the sum of all individual decay rates, $\Gamma = \sum_j \Gamma_j$. In our system of natural units, the dimension of Γ is equivalent to mass (or energy) as it is the inverse of time. As expected, the mass of the charged Higgs boson increases with increasing neutral Higgs mass m_{ϕ^0} under all circumstances. The decay widths are highly sensitive to the mass hierarchy and mass splitting. Shrinking of the decay width is observed when $m_{H^0} - m_{H^\pm}$, the mass splitting is minimal, as shown in Figure 4. The decay width for BP-1 decreases from 8.66 to 1.42 when the m_{H^\pm} goes from 379 to 691 GeV . For BP-2, the decay width increases from 4.38 to 5.22 for m_{H^\pm} in the range of $250 < m_{H^\pm} < 550$ GeV . The Γ_{H^\pm} for BP-3 increases from 3.5×10^{-5} to 4.28 when m_{H^\pm} runs from 48.75 to 436 GeV . For the last BP-4, the decay width decreases from 60 to 58 for change of m_{H^\pm} from 558 to 564 GeV .

The BR (or branching fraction) is the proportional frequency of a particular decay mode. The BR

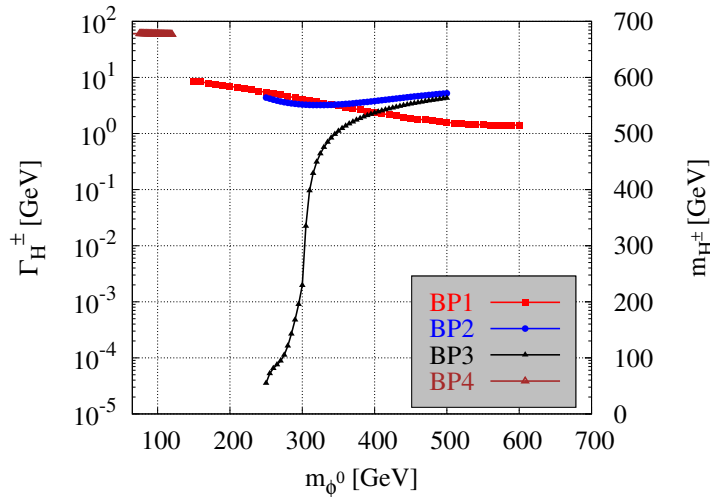


FIG. 4: Total decay widths for charged Higgs boson H^\pm for all benchmark points.

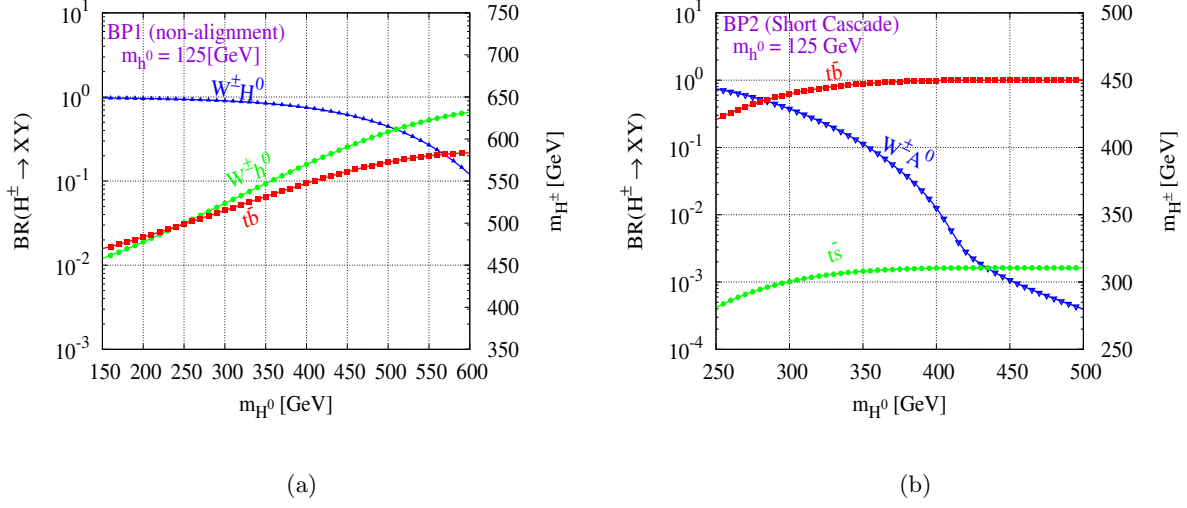


FIG. 5: The BR of H^\pm predicted in BP-1 from (a) and BP-2 in (b), respectively. For modes, BR is less than 10^{-4} are omitted for clarity.

is the decay rate to the specific mode i.e. j relative to the total decay rate.

$$BR(j) = \frac{\Gamma_j}{\Gamma}$$

Here Γ is the total decay width and Γ_j is the partial decay width i.e. decay width of an individual particle. We showed the dominant modes of BR for H^\pm as function of h^0 and H^0 , for all scenarios. The $W^\pm H^0$ channel is the primary decay mode for H^\pm in BP-1, as shown in Figure 5. The sub-dominant channels are as follows: $t\bar{b}$ and $W^\pm h^0$ for charged Higgs for BP-1, other

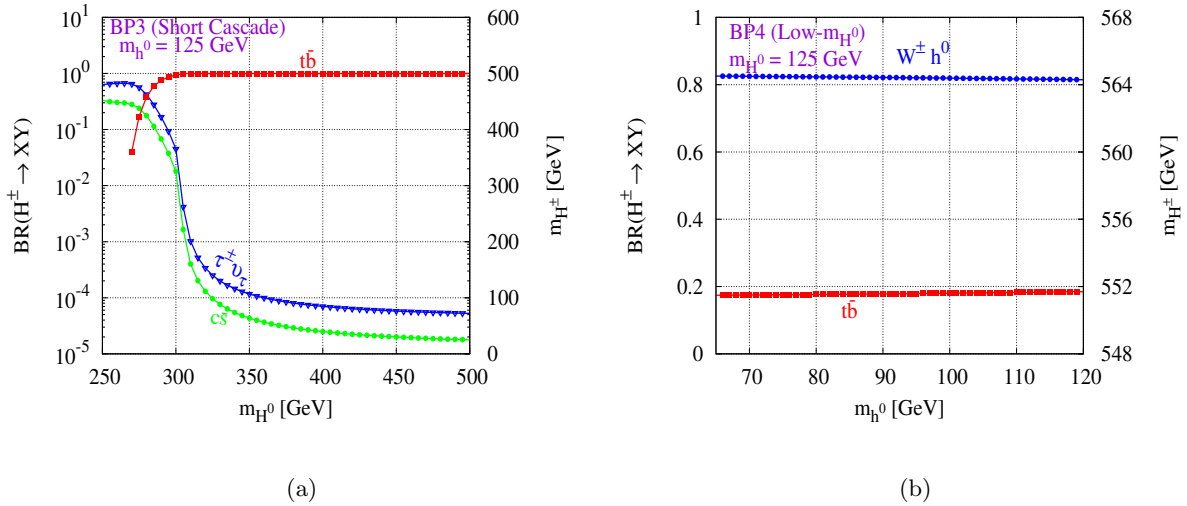


FIG. 6: The BR of H^\pm predicted in BP-3 from (a) and BP-4 in (b), respectively. For modes, BR is less than 10^{-4} are omitted for clarity.

suppressed channels are $c\bar{s}$ and $t\bar{s}$ for range $m_{H^0} < 500 \text{ GeV}$. The mode of decay $W^\pm h^0$ takes control when $BR(H^\pm \rightarrow W^\pm H^0)$ decreases at larger values of m_{H^0} . So for $BR(H^\pm \rightarrow W^\pm h^0)$ range rises from 1.2 to 66.3% of $150 < m_{H^0} < 600 \text{ GeV}$. The process H^0 to W^+W^- is also another dominant decay mode with BR of 88.7 to 50.2% and with hadronic decay of W^\pm has 12-jets in the final state.

In the BP-2 and BP-3 as shown in Figure 5 and Figure 6 respectively, as $m_{H^\pm} > m_t + m_b$ the BR of 100% prominent decay mode is $H^\pm \rightarrow t\bar{b}$. The suppressed decay modes of $m_{H^0} < 300 \text{ GeV}$ are for $W^\pm A^0$ and $t\bar{s}$ in both BP-2 and BP-3; the t -quark decay is an ideal for the reconstruction of the process at $m_{H^0} > 300 \text{ GeV}$. So for process $t \rightarrow Wb, W \rightarrow q\bar{q}(l\nu_l)$ gives H^\pm trace at the detector which can be tagged with 8-jets and 2-b-tagged jets.

For BP-4, shown in Figure 6, for a range of $65 < m_{h^0} < 120 \text{ GeV}$ the dominant channel is $W^\pm h^0$ because for $\sin(\beta - \alpha) = 0$ it leads to 100%. 4-jets and 4-b-tagged jets can be used to tag the process.

VIII. MULTIVARIATE ANALYSIS FOR CHARGED HIGGS PRODUCTION

An integrated ROOT framework for parallel running and computation of several multivariate categorization algorithms is called the ‘‘Toolkit for Multivariate Analysis’’ [39], which categorizes using two sorts of events: signal and background. TMVA especially has many applications in high energy physics for the complex multiparticle final state. To train the classifiers, a set of events with well-defined event types is inserted into the Factory. The event samples for signal and background can either be read using a tree-like structure or a plain text file using a defined structure. All variables that are supposed to separate signal and background events must be known by the Factory. Cuts are applied on signal and background trees separately.

We represent three classifiers in our work; Boosted Decision Tree (BDT), LikelihoodD (Decorrelation), and MLP. In BDT a selection Tree is a tree-like structure that illustrates the different outcomes of a choice using a branching mechanism. An event is categorized as either a signal or a background event by passing or failing to pass a condition (cut) on a certain node until a choice is reached. The ‘‘root node’’ of the decision tree is used to find these cuts. The node-splitting process concludes when the BDT algorithm specifies minimal events (`NEventsMin`). The final nodes (leaves) are classified according to their ‘‘purity’’ (p). The value for signal or background (usually +1 for signal and 0 or -1 for background) depends on whether p is greater than or less than the stated number, e.g. +1 if $p > 0.5$ and -1 if $p < 0.5$ [40]. To differentiate between the

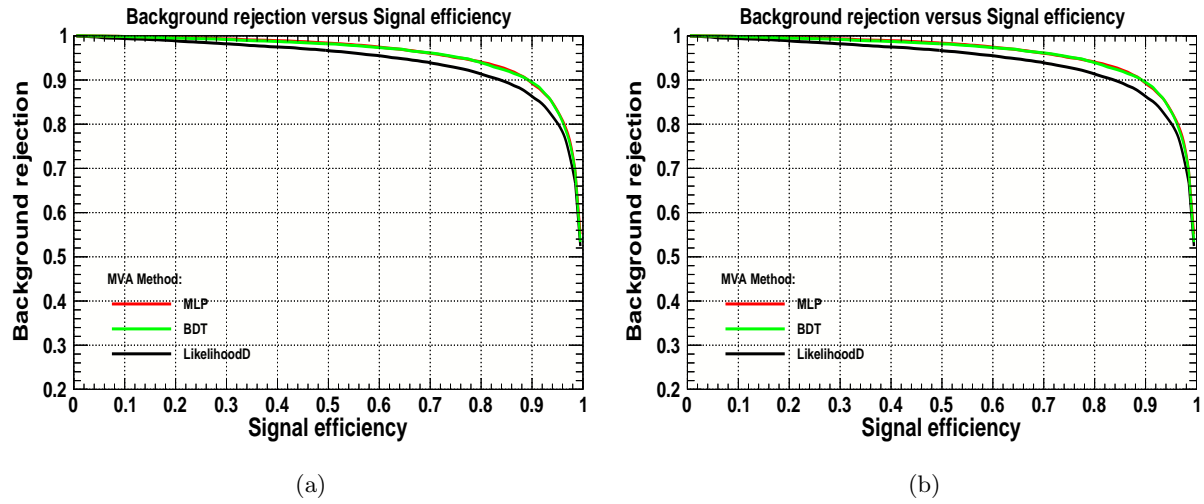


FIG. 7: Background Rejection vs Signal Efficiency with applying cuts (a) and without applying cuts (b), respectively.

background class and signal, a labeling process is carried out. All occurrences with a classifier output $y > y_{cut}$ are labeled as a signal, while the rest are classified as background. The purity of the signal efficiency $\epsilon_{sig,eff}$, and background rejection ($1 - \epsilon_{bg,eff}$) are evaluated for each cut value of y_{cut} [41]. ADA-Boost algorithm re-weights every misclassified event candidate. The new candidate weight consists of the one used in the former tree multiplied by $\alpha = 1 - \Delta_m/\Delta_m$, where Δ_m is the misclassification error. This leads to an increase in the weight and therefore an increase in the candidate's importance when searching for the best separation values. The weights of each new tree are based on the ones of its predecessor [42]. An Artificial Neural Network (ANN) comprises linked neurons, each with its weight. To speed up the processing, a reduced layout can be used as well, the so-called multilayer perceptron (MLP). The network consists of three kinds of layers. The input layer, consisting of n_{var} neurons and a bias neuron, many deep layers containing a user-specified number of neurons (set in the option `HiddenLayers`) plus a bias node, and an

MVA Classifier	AUC (with cut)	AUC (without cut)
MLP	0.958	0.922
BDT	0.957	0.925
LikelihoodD	0.941	0.896

TABLE IV: MVA Classifier Area Under (AUC) the Curve with cuts and without cuts values

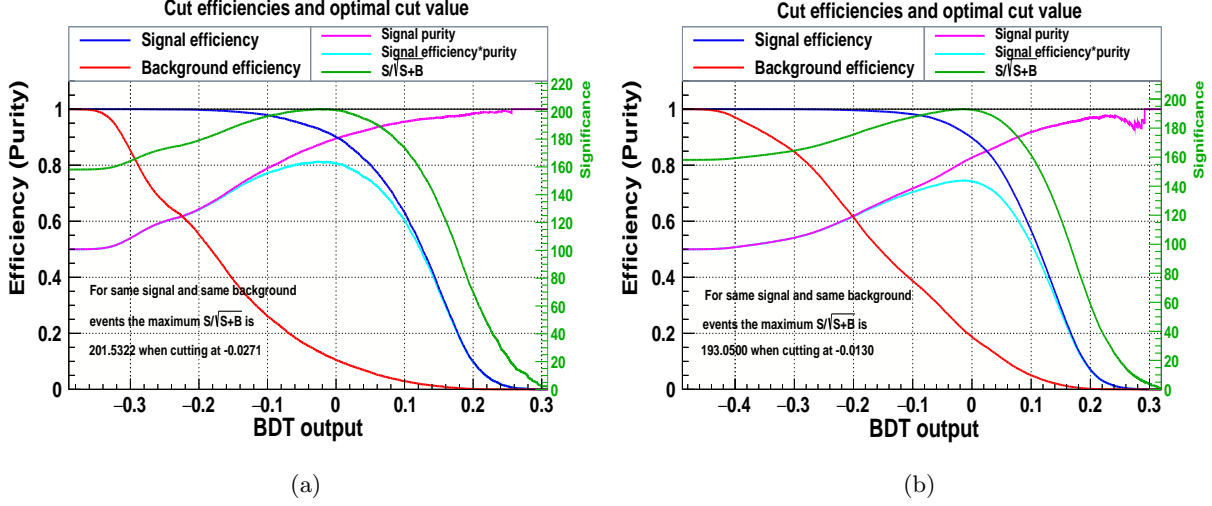


FIG. 8: BDT signal significance with applying cuts (a) and without applying cuts (b) respectively.

output layer and each of the connection between two neurons carries a weight.

For event j , the likelihood ratio $y_L(j)$ is defined by

$$y_L(j) = \frac{L_S(j)}{L_S(j) + L_B(j)} \quad (25)$$

where the likelihood of a candidate to be signal/background may be determined using the following formula

$$L_{S/B}(j) = \prod_{i=1}^{n_{var}} P_{S/B,i}(x_i(j)) \quad (26)$$

where $P_{S/B,i}$ is the PDF for the i th input variable x_i . The PDFs are normalized to one for all i :

$$\int_{-\infty}^{\infty} P_{S/B,i}(x_i) dx_i = 1 \quad (27)$$

The projective likelihood classifier has a major drawback in that it does not use correlation among the discriminating input variables. In the realistic approach, it does not provide an accurate analysis and leads to performance loss. Even other classifiers underperform in the presence of variable correlation. Linear Correlation was used to quantify the training sample by obtaining the square root of the covariant matrix. The square root of the matrix C is C' , which when multiplied by itself yields $C : C = (C')^2$. As a result, TMVA employs diagonalization of the (symmetric) covariance matrix provided by:

$$D = S^T C S \implies C' = S \sqrt{D} S^T \quad (28)$$

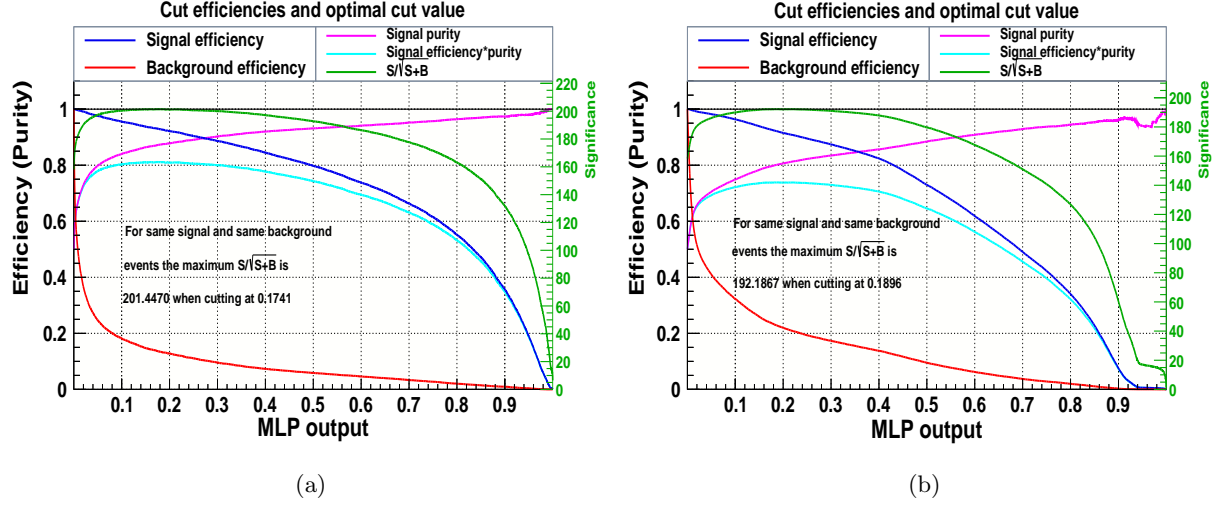


FIG. 9: MLP Signal Significance with applying cuts (a) and without applying cuts (b) respectively.

D is the diagonal matrix, while S denotes the symmetric matrix. The linear decorrelation is calculated by multiplying the starting variable \mathbf{x} by the inverse of C' .

$$\mathbf{x} \mapsto (C')^{-1}\mathbf{x} \quad (29)$$

Only linearly coupled and Gaussian distributed variables have full decorrelation. In this work, the signal and background events are taken to be 50000 with applied cuts:

$$P_T^{Jet} > 30 \text{ GeV} , \quad \eta_{Jet} < 2 , \quad N_{Jet} \leq 6 , \quad \Delta R < 0.4 , \quad E_T^{Missing} < 120 \text{ GeV}$$

The curve of background rejection against signal efficiency provides a reasonable estimate of a classifier's performance. A classifier's performance is measured by the area under the signal efficiency versus the background rejection curve, so the bigger the area, the better a classifier's predicted separation power, as shown in Figure 7. The values of area under the curve (AUC) for

MVA Classifier	Signal Significance (with cuts)	Signal Significance (without cuts)
MLP	201.44	192.187
LikelihoodD	198.658	188.409
BDT	201.532	193.05

TABLE V: The signal significance for the classifiers of signal and background with applied cuts and without applied cuts.

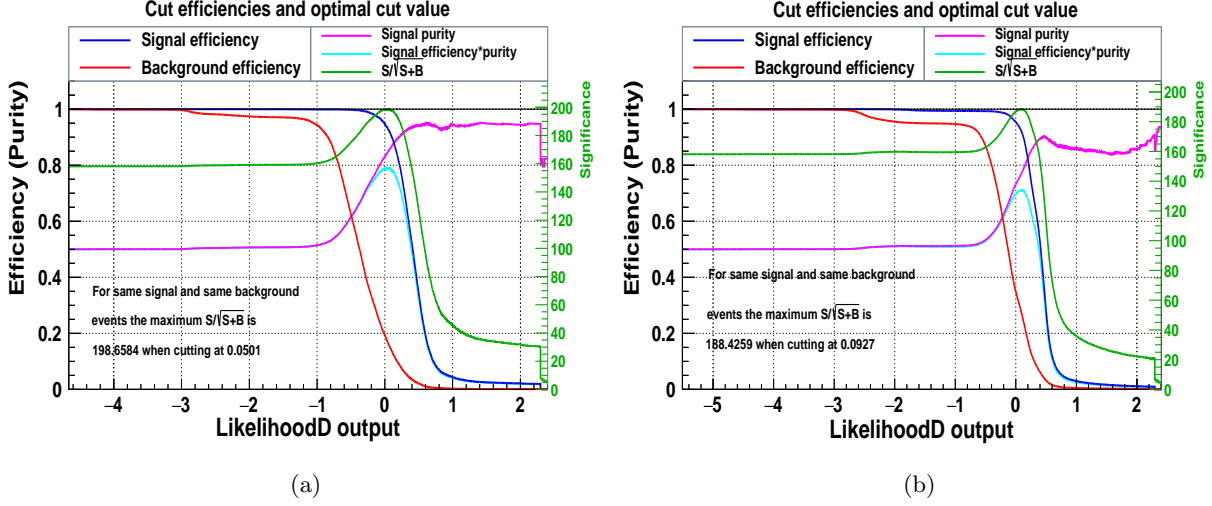


FIG. 10: LikelihoodD Signal Significance with applying cuts (a) and without applied cuts (b) respectively.

Figure 7. Table IV shows that the best classifier among all is the MLP and BDT, improved after applying cuts and gave the largest area under the curve.

We used 800 trees to improve the BDT's performance, with node splitting at 2.5% event threshold. Max tree depth set at 3. Trained using Adaptive Boost with a learning rate of $\beta = 0.5$ parent node and the sum of the indices of the two daughter nodes are compared to optimize the cut value on the variable in a node. For the separation index, we use the *Gini Index*. Finally, the variable's range is evenly graded into 20 cells. The signal values are taken to be 1 and background values approach to 0. Figure 8 depicts that the signal significance, $S/\sqrt{S+B}$, of the classifier, is improved by applying cuts with an optimal cut of -0.0271. Similarly, Figure 9 shows the best classifier that is improved by applying cuts with an optimal cut value of 0.1741, and the signal efficiency is also higher than without applied cuts. The LikelihoodD signal significance is shown in Figure 10, has been improved by applied cuts with the optimal cut of 0.0501.

IX. CONCLUSION

The simplest extension of SM is 2HDM containing charged Higgs Boson and the exact measurement of its nature corresponding model parameters are crucial for the discovery. The pair production is one of the best channels that provided the observable signal in the vast range of parameters in 2HDM.

The generation rates of incoming beams are investigated in various polarization collision patterns. The cross-section can be increased twice by oppositely polarized beams of photons at

high energies and right-handed polarized beams of photons at low energies as shown in the figures of the cross-section. For BP-1 at the $\sqrt{s} = 3 \text{ TeV}$ the $\sigma^{UU} = 12.92 \pm 8.1 \times 10^{-06}$ fb, for $\sigma^{RR} = 0.3568 \pm 4.6 \times 10^{-07}$ fb and for $\sigma^{RL} = 25.48 \pm 1.6 \times 10^{-05}$ fb. For BP-2 the cross section for $\sigma^{UU} = 12.76 \pm 8.03 \times 10^{-06}$ fb, $\sigma^{RR} = 0.4067 \pm 5.3 \times 10^{-07}$ fb and for $\sigma^{RL} = 25.11 \pm 1.8 \times 10^{-05}$ fb at the center of mass energy 3 TeV . The cross section at 3 TeV for BP-3 for different polarizations are $\sigma^{UU} = 13.22 \pm 9.1 \times 10^{-06}$ fb, $\sigma^{RR} = 0.2674 \pm 3.2 \times 10^{-07}$ fb and $\sigma^{RL} = 26.17 \pm 1.7 \times 10^{-05}$ fb respectively. The Low- m_H scenario for BP-4 the cross section for polarized beams are $\sigma^{UU} = 13.23 \pm 9.1 \times 10^{-06}$ fb, $\sigma^{RR} = 0.2673 \pm 3.2 \times 10^{-07}$ fb and for $\sigma^{RL} = 26.19 \pm 1.7 \times 10^{-05}$ fb at $\sqrt{s} = 3 \text{ TeV}$ respectively. So we concluded that for all BP's, the cross-section is low at high energy for UU and RR polarized beams of photons, while high for RL at high energy.

For each scenario, the charged Higgs Boson reconstruction has been provided, and its prominent decay modes have been examined. The branching ratio of the decay channel for non-alignment, the bosonic decay channel $H^\pm \rightarrow W^\pm H^0$ is the dominant while in the low- m_H scenarios the bosonic decay of $W^\pm h^0$ is dominant rises to 66.3%. The 100% dominant decay channel in a short-cascade scenario is $H^\pm \rightarrow t\bar{b}$ that concludes the t decay is the ideal candidate for the reconstruction of the process. Limited phase space and alignment constraints restrict bosonic decay channels.

Our Machine Learning models for Multivariate Analysis results are improved by applying cuts. The signal efficiency ($\epsilon_{Sig,eff}$) and background rejection ($1 - \epsilon_{Bkg,eff}$) are increased when cuts are applied to the MLP, BDT, and LikelihoodD classifiers. The area under the curve (AUC) is increased for MLP to 3.9%, for BDT increased to 3.46%, and the LikelihoodD increased up to 5.02% which shows that the LikelihoodD is the more efficient classifier for signal efficiency and background rejection. The signal significance is increased for MLP to 4.81%, for the BDT increased to 4.39%, and for LikelihoodD, it is increased to 5.43% by applying cuts. The significance values obtained with cuts demonstrate how well these models can separate charged Higgs production-related background events from signal occurrences. These cuts most likely aid in lowering background noise, enhancing overall performance, and separating signal events associated with charged Higgs generation. This consistency upholds the validity of the selected machine-learning approaches and increases trust in the outcomes.

X. ACKNOWLEDGEMENTS

We gratefully acknowledge support from the Simons Foundation and member institutions. The current submitted version of the manuscript is available on the arXiv pre-prints home page

XI. STATEMENTS AND DECLARATIONS

Funding The authors declare that no funds, grants, or other support were received during the preparation of this manuscript.

Competing Interests The authors have no relevant financial or non-financial interests to disclose.

Availability of data and materials Data sharing does not apply to this article as no datasets were generated or analyzed during the current study.

-
- [1] Observation of a new particle in the search for the Standard Model Higgs boson with the ATLAS detector at the LHC, ATLAS, Collaboration, arXiv preprint arXiv:1207.7214, (2012)
 - [2] Observation of a new boson at a mass of 125 GeV with the CMS experiment at the LHC, CMS Collaboration, arXiv preprint arXiv:1207.7235, (2012)
 - [3] Precise determination of the mass of the Higgs boson and tests of compatibility of its couplings with the standard model predictions using proton collisions at 7 and 8 TeV, Collaboration, CMS, Eur. Phys. J. C, (2015)
 - [4] Prospects for charged Higgs searches at the LHC., Arhrib, A and Hernandez-Sanchez, J and Mahmoudi, F and Santos, R and Akeroyd, A and Moretti, S and Yagyu, K and Yildirim, E and Khater, W and Krawczyk, M and others, European Physical Journal C–Particles & Fields, (2017)
 - [5] Neutral currents and the Higgs mechanism, Ross, DA and Veltman, M, Nuclear Physics B, (1975)
 - [6] Second threshold in weak interactions, Veltman, MJG, Acta Phys. Pol. B, (1976)
 - [7] Limit on mass differences in the Weinberg model, Veltman, M, Nuclear Physics B, (1977)
 - [8] Study of $(W/Z)H$ production and Higgs boson couplings using $H \rightarrow WW^*$ decays with the ATLAS detector, ATLAS collaboration and others, arXiv preprint arXiv:1506.06641, (2015)
 - [9] Combined Measurement of the Higgs Boson Mass in pp Collisions at $\sqrt{s} = 7$ and 8 TeV with the ATLAS and CMS Experiments, Collaborations, CMS, and others, arXiv preprint arXiv:1503.07589, (2015)
 - [10] Charged Higgs pair production in a general two Higgs doublet model at e^+e^- and $\mu^+\mu^-$ linear colliders, author=Hashemi, Majid, Communications in Theoretical Physics, (2014)
 - [11] Yukawa corrections to charged Higgs-boson pair production in photon-photon collisions, Ma, Wen-Gan and Li, Chong Sheng and Liang, Han, Physical Review D, (1996)

- [12] Erratum to New LHC benchmarks for the CP-conserving two-Higgs-doublet model, Haber, Howard E and Stål, Oscar, The European Physical Journal C, (2016)
- [13] Searching for signs of the second Higgs doublet, Craig, Nathaniel and Galloway, Jamison and Thomas, Scott, arXiv preprint arXiv:1305.2424, (2013)
- [14] Natural conservation laws for neutral currents, Glashow, Sheldon L, and Weinberg, Steven, Physical Review D, (1977)
- [15] Diagonal neutral currents, Paschos, Emmanuel A, Physical Review D, (1977)
- [16] Theory and phenomenology of two-Higgs-doublet models, Branco, Gustavo Castelo and Ferreira, PM and Lavoura, L and Rebelo, MN and Sher, Marc and Silva, Joao P, Physics reports, (2012)
- [17] PRINT-86-1324 (UC, DAVIS); JF Gunion, HE Haber, GL Kane and S. Dawson, Gunion, John F and Kayser, B, and Mohapatra, RN and Deshpande, NG and Grifols, J and Mendez, A and Olness, FI and Pal, PB, Front. Phys, (2000)
- [18] Pattern of symmetry breaking with two Higgs doublets, Deshpande, Nilendra G and Ma, Ernest, Physical Review D, (1978)
- [19] Search for microscopic black hole signatures at the Large Hadron Collider, CMS collaboration and others, arXiv preprint arXiv:1012.3375, (2010)
- [20] The global electroweak fit at NNLO and prospects for the LHC and ILC, Gfitter Group and Baak, M, and Cúth, J and Haller, J and Hoecker, A and Kogler, Roman and Mönig, K and Schott, M and Stelzer, J, The European Physical Journal C, (2014)
- [21] Search for heavy ZZ resonances in the final states using proton-proton collisions at TeV with the ATLAS detector, Aaboud, M and Aad, G and Abbott, B and Abeloos, B and Abidi, SH and AbouZeid, OS and Abraham, NL and Abramowicz, H and Abreu, H and Abreu, R and others, The European Physical Journal. C, Particles, and fields, (2018)
- [22] collisions at $\sqrt{s} = 8$ TeV with the ATLAS detector. Physics Letters B, 744, pp. 163-183. Copyright© 2015 CERN, for the ATLAS Collaboration., Aad, G, and others, Physics Letters B, (2015)
- [23] Measurements of the Higgs boson production and decay rates and coupling strengths using pp collision data at $\sqrt{s} = 7$ and 8 TeV in the ATLAS experiment, Aad, Georges and Abbott, Brad and Abdallah, Jalal, and Aben, R and Abolins, M and AbouZeid, OS and Abramowicz, H and Abreu, H and Abreu, R and Abulaiti, Y and others, The European Physical Journal C, (2016)
- [24] Updated next-to-next-to-leading-order QCD predictions for the weak radiative B-meson decays, Misiak, M and Asatrian, HM, Boughezal, Radja and Czakon, M and Ewerth, T and Ferroglia, A. and Fiedler, P. and Gambino, Paolo and Greub, Christoph and Haisch, U, and others, Physical review letters, (2015)
- [25] Weak radiative decays of the B meson and bounds on M_H^\pm in the Two-Higgs-Doublet Model, Misiak, Miłkołaj and Steinhauser, Matthias, The European Physical Journal C, (2017)
- [26] Unitarity bound in the most general two Higgs doublet model, Kanemura, Shinya and Yagyu, Kei, Physics Letters B, (2015)
- [27] Flavor constraints on the two Higgs doublet models of Z_2 symmetric and aligned types, Enomoto,

- Tetsuya and Watanabe, Ryoutaro, *Journal of High Energy Physics*, (2016)
- [28] Bosonic decays of charged Higgs bosons in a 2HDM type-I, Arhrib, Abdesslam and Benbrik, Rachid and Moretti, Stefano, *The European Physical Journal C*, (2017)
 - [29] Search for charged Higgs bosons decaying via $H^\pm \rightarrow \tau^\pm \nu$ in fully hadronic final states using pp collision data at $\sqrt{s} = 8$ TeV with the ATLAS detector, Aad, Georges Abbott, B. and Abdallah, J and Abdel Khalek, S and Aben, R. and Abi, B. and Abolins, M and AbouZeid, OS and Abramowicz, H and Abreu, H and others, *Journal of High Energy Physics*, (2015)
 - [30] Search for a charged Higgs boson in pp collisions at $\sqrt{s} = 8$ TeV, Khachatryan, Vardan and Sirunyan, Albert M and Tumasyan, Armen and Adam, Wolfgang and Asilar, E and Bergauer, Thomas and Brandstetter, Johannes and Brondolin, Erica and Dragicevic, Marko and Erö, Janos and others, *Journal of High Energy Physics*, (2015)
 - [31] Search for a light-charged Higgs boson in the decay channel $H^\pm \rightarrow c(s)$ over-bar in $t(t)$ over-bar events using pp collisions at $\sqrt{s} = 7$ TeV with the ATLAS detector, Aad, G and Borjanović, Iris and Božović-Jelisavčić, Ivanka and Ćirković, Predrag and Agatonović-Jovin, Tatjana and Krstić, Jelena and Mamužić, Judita and Popović, DS and Sijackii, Dj and Simić, Lj and others, *European Physical Journal C. Particles and Fields*, (2013)
 - [32] Search for charged Higgs bosons: combined results using LEP data, ALEPH Collaboration, DELPHI Collaboration, L3 Collaboration, OPAL Collaboration, and LEP working group for Higgs boson searches, *The European Physical Journal C*, (2013)
 - [33] Prospects for charged Higgs searches at the LHC, Akeroyd, AG and Aoki, M and Arhrib, A and Basso, L and Ginzburg, IF and Guedes, R and Hernandez-Sanchez, J and Huitu, K and Hurth, T and Kadastik, M and others, *The European Physical Journal C*, (2017)
 - [34] 2HDMC—two-Higgs-doublet model calculator, Eriksson, David and Rathsmann, Johan and Stål, Oscar, *Computer Physics Communications*, (2010)
 - [35] Problems in obtaining $\gamma\gamma$ and γe colliding beams at linear colliders, Telnov, Valery I, *Nuclear Instruments and Methods in Physics Research Section A: Accelerators, Spectrometers, Detectors and Associated Equipment*, (1990)
 - [36] MadGraph 5: going beyond, Alwall, Johan and Herquet, Michel and Maltoni, Fabio and Mattelaer, Olivier and Stelzer, Tim, *Journal of High Energy Physics*, (2011)
 - [37] 2HDMC—a two Higgs doublet model calculator, Rathsmann, Johan and Stål, Oscar, *arXiv preprint arXiv:1104.5563*, (2011)
 - [38] gnuplot 4.6, Williams, Thomas and Kelley, Colin and Bröcker, Hans-Bernhard and Campbell, John and Cunningham, Robert and Denholm, David and Elber, Gershon and Fearick, Roger and Grammes, Carsten and Hart, Lucas and others, *An Interactive Plotting Program*, (2012)
 - [39] ROOT—An object-oriented data analysis framework, Brun, Rene and Rademakers, Fons, *Nuclear instruments and methods in physics research section A: accelerators, spectrometers, detectors and associated equipment*, 1997

- [40] Boosted decision trees, Coadou, Yann, Artificial Intelligence for High Energy Physics, (2022)
- [41] The toolkit for multivariate data analysis, TMVA 4, Speckmayer, P, and Höcker, A and Stelzer, J and Voss, H, Journal of Physics: Conference Series, (2010)
- [42] An introduction to boosting and leveraging, Meir, Ron and Rätsch, Gunnar, Advanced Lectures on Machine Learning: Machine Learning Summer School 2002 Canberra, Australia, February 11–22, 2002 Revised Lectures, (2003)